

the rate-controlling step does not involve solvation or that H₂O partitions so strongly into the mineral interface that its concentration at the interface is not greatly affected by 95 percent dilution in the bulk of the fluid. In either case, the result greatly extends the applicability of the observed rate relation. A similar conclusion applies to the effect of total pressure; we find no systematic effect of total pressure on rate constants at pressures from 1 to 7000 bar. Thus, it appears that temperature dominates over fluid composition and pressure effects in the single-crystal studies.

The solid line in Fig. 2 describes a rate constant given by the equation

$$\log k \approx -2900/T - 6.85 \quad (5)$$

where T is temperature and where k has the units gram-atoms of oxygen per square centimeter per second. The possible applications of this expression to geologic phenomena are many, but let us consider as an example a prograde metamorphic dehydration reaction with $\Delta S_r = 80 \text{ J K}^{-1}$. At 500°C overstep of this reaction boundary by 1°C with 2-mm crystals would cause the reaction to go to completion in 330 years, given the presence of all phases involved. At 700°C the reaction would go to completion in 70 years. These rapid rates support the classic observation (28) that prograde mineral assemblages remain very close to thermodynamic equilibrium when a fluid phase is present.

BERNARD J. WOOD
JOHN V. WALTHER

Department of Geological Sciences,
Northwestern University,
Evanston, Illinois 60201

References and Notes

- M. Lagache, *Bull. Soc. Fr. Mineral. Cristallogr.* **88**, 223 (1965).
- W. S. Fyfe, *Geochim. Cosmochim. Acta* **40**, 157 (1976).
- E. Busenburg and C. V. Clemency, *ibid.*, p. 41.
- G. R. Holden, Jr., and R. A. Berner, *ibid.* **43**, 1161 (1979).
- F.-C. Lin and C. V. Clemency, *ibid.* **45**, 571 (1981).
- W. S. Fyfe, *Clays Clay Miner.* **29**, 101 (1981).
- J. D. Rimstidt and H. L. Barnes, *Geochim. Cosmochim. Acta* **44**, 1683 (1980).
- W. S. Fyfe and M. A. Hollander, *Am. J. Sci.* **262**, 709 (1964).
- B. W. Evans, *ibid.* **263**, 647 (1965).
- M. J. Holdaway, *ibid.* **264**, 643 (1966).
- D. M. Kerrick, *ibid.* **266**, 204 (1968).
- A. B. Thompson, *ibid.* **269**, 267 (1970).
- A. B. Thompson, *ibid.* **271**, 72 (1971).
- M. J. Holdaway, *ibid.*, p. 97.
- D. M. Kerrick, *ibid.* **272**, 946 (1972).
- H. H. Haas and M. J. Holdaway, *ibid.* **273**, 449 (1973).
- N. D. Chatterjee and W. Johannes, *Contrib. Mineral. Petrol.* **48**, 89 (1974).
- J. Slaughter, D. M. Kerrick, V. J. Wall, *Am. J. Sci.* **275**, 143 (1975).
- A. B. Thompson, in *Progress in Experimental Petrology*, G. M. Biggar, Ed. (Natural Environment Research Council, London, 1976), p. 9.
- P. Aagaard and H. C. Helgeson, *Am. J. Sci.* **282**, 237 (1982).
- J. Schott, R. A. Berner, E. L. Sjöberg, *Geochim. Cosmochim. Acta* **45**, 2123 (1981).
- W. S. Fyfe, *J. Geol.* **68**, 553 (1960).
- A. C. Lasaga and G. W. Fisher, in *Kinetics of Geochemical Processes*, A. C. Lasaga and R. J. Kirkpatrick, Eds. (Mineralogical Society of America, Washington, D.C., 1981), p. 135.
- H. Eyring, *J. Chem. Phys.* **3**, 107 (1935).
- M. Boudart, *J. Phys. Chem.* **80**, 2869 (1976).
- H. C. Helgeson, J. M. Delany, H. W. Nesbitt, D. K. Bird, *Am. J. Sci.* **278A**, 1 (1978).
- R. Wollast, personal communication.
- V. M. Goldschmidt, *Z. Anorg. Chem.* **71**, 313 (1911).
- Supported by NSF grants EAR80-24146 and 82-12502.

17 January 1983; accepted 23 June 1983

Electron Density Distribution in the Organic Superconductor (TMTSF)₂AsF₆

Abstract. Excellent crystals of (TMTSF)₂AsF₆ (TMTSF, tetramethyltetraselenafulvalene) were employed to obtain x-ray diffraction data for a determination of the electron density distribution in this organic superconductor. Electron density was observed between molecules in a stack of donors of an organic metal and between certain interstack selenium atoms of these donors.

Certain organic molecules give rise to organic metals when converted to radical ions. (1). These organic solids conduct electricity preferentially in one direction, usually along the long axis of the needle-shaped crystals. Most organic molecules that form organic metals are planar, are of D_{2h} symmetry, and pack most efficiently in stacks like a deck of cards. The stacking direction corresponds to the long crystal axis mentioned above. Since in most organic metals approximately 50 percent of the molecules in a stack are charged, there is a definite ionic contribution to the lattice energy. However,

there are still questions regarding cohesive forces in these salts (2)—for example, how much the metal-band electrons contribute to lattice binding energies, and whether these electrons contribute mostly by screening Coulombic repulsive forces (3).

The high conductivities observed along the stacking direction of organic metals are assumed to be due to the existence of intrastack bonding. In the first organic metal, tetrathiafulvalenium tetracyanoquinodimethanide (TTF-TCNQ), intermolecular intrastack bonding was inferred from comparisons of intermolecular intrastack distances in the neutral component molecules (for example, 3.62 Å in TTF-TTF and 3.45 Å in TCNQ-TCNQ) with the same intermolecular distances in TTF-TCNQ (3.47 Å in TTF-TTF and 3.17 Å in TCNQ-TCNQ). It was clearly of interest to determine the actual electron density distribution in an organic metal.

Recently, x-ray diffraction alone rather than combined x-ray and neutron diffraction has been used for experimental electron density studies (4–7). Experience has shown that to obtain meaningful electron density maps the crystals must be of excellent quality (6, 7). Such crystals were unavailable for the TCNQ-based metals (TTF-TCNQ, TSF-TCNQ, and so on) or TTF-based metals [TTFI_n, TTF(SeCN)_n], but were found for a family of the tetramethyltetraselenafulvalene (TMTSF) donor [(TMTSF)₂X, where X is an octahedral or tetrahedral complex univalent anion]. Wudl (8) reported that (TMTSF)₂AsF₆ forms nearly perfect crystals and suggested several interstack and intrastack selenium-selenium “bonding” interactions. The validity of these suggestions could be tested only through experimental electron density determinations.

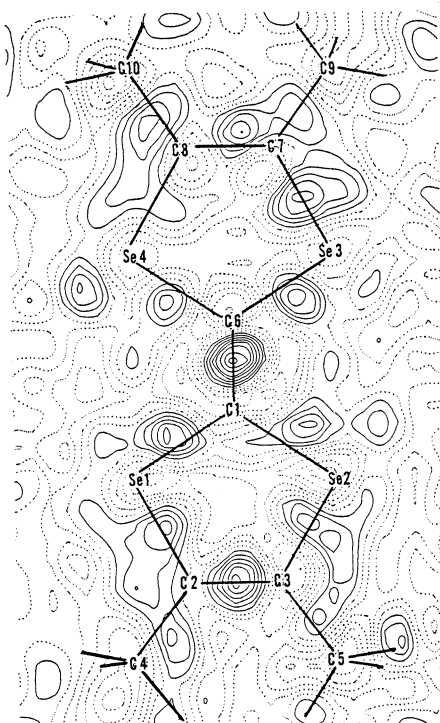


Fig. 1. Electron densities in the plane of a TMTSF molecule. Contours are 0.05 $e/\text{\AA}^3$ per contour line starting at 0.05 $e/\text{\AA}^3$; negative contours are shown by broken lines and the error is 0.05 $e/\text{\AA}^3$ for all density maps.

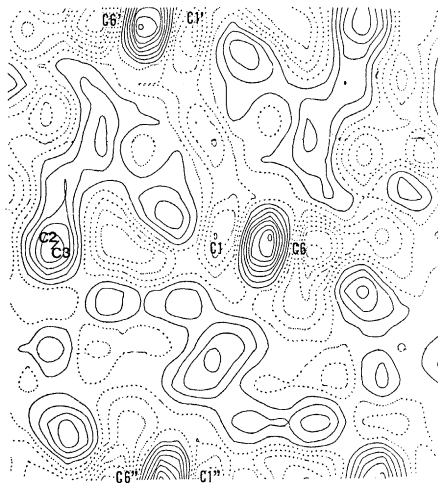


Fig. 2. Electron density "slices" through the centers of TMTSF molecules along the TMTSF stack. Primes are related by symmetry code (-111). Double primes are related by symmetry code (-121). See Table 1 for explanation of symmetry codes.

In this report we describe the experimental observation of significant electron density between molecules in an organic metal (9).

The structure was solved by using atomic coordinates from a previous structure solution (8). Atomic coordinates, bond distances, and bond angles agreed within 3 standard deviations with the previous structure determination. In addition, crystals of $(\text{TMTSF})_2\text{PF}_6$ and $(\text{TMTSF})_2\text{AsF}_6$ were studied by taking numerous data sets with redundant data both at room temperature ($\sim 25^\circ\text{C}$) and at -113°C . Both compounds have residual peaks above and below the plane of selenium atoms at low temperatures, presumably due to a slight static disorder resulting from a minor phase change.

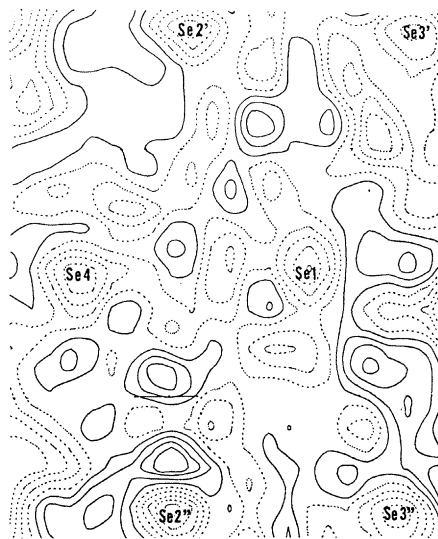


Fig. 3. Electron density slice through the selenium atoms of TMTSF molecules along a stack edge. See Fig. 2 legend for details.

This was reflected largely as a 1° change in one of the unit cell angles and a contraction in the a cell dimension, which is aligned with the stacking direction at low temperatures. The room-temperature study for the AsF_6 salt gave the best refinement (10) and electron density maps and is therefore reported here. The results of the electron density study of the PF_6 salt are in qualitative agreement with those for the AsF_6 salt.

Electron density maps were calculated following a limited high-angle refinement where only data for $\sin \theta/\lambda > 0.55 \text{ \AA}^{-1}$ were used; this was a consequence of minimal high-angle scattering, presumably due to a $1/3$ - $2/3$ rotational disorder observed in the AsF_6 groups. Only the selenium and carbon atoms were refined, and the disordered AsF_6 , hydrogen atoms, extinction parameters, and scale factor were held constant at full-angle refinement values (11). Deformation maps were prepared with data for $\sin \theta/\lambda < 0.60 \text{ \AA}^{-1}$ to eliminate accumulated errors from the higher angle data. This technique has also been used successfully for $(\text{CH}_3)_2\text{TeCl}_2$ (5, 7). The error in the electron density away from atom centers is calculated based on σF as $0.05 e/\text{\AA}^3$, where F is structure factor. The error within 0.4 \AA of atom centers is high, primarily because of errors in thermal parameters (12).

Representative electron density maps are shown in Figs. 1 through 4. These include densities in the TMTSF plane and several other intrastack and interstack planes.

The electron density was observed to be highest for the C2-C3 and C1-C6 double bonds and lower for the C7-C8 double bond (Fig. 1), in line with observed bond lengths (8). With the exception of Se4, there is little selenium lone-pair density in the TMTSF plane, implying that the selenium atoms are not sp^2 hybridized (13). In fact, the lone-pair density appears in a tetrahedral arrangement with respect to the selenium atoms and is highest about 0.6 \AA above and below the TMTSF plane (11), corroborating the suggestion that the selenium atoms may be sp^3 hybridized (13). An accumulation of density between Se4 and Se3 as well as between Se1 and Se2, was also observed above and below the TMTSF plane, implying the existence of some transannular bonding between selenium atoms, probably through the back lobes of an $sp^n (n \neq 2)$ hybrid (14).

The $(\text{TMTSF})_2\text{X}$ phase consists of stacks of TMTSF molecules and sheets of anions, with the highest conductivity observed along the a axis (stacking axis). Since substantial conductivity is also ob-

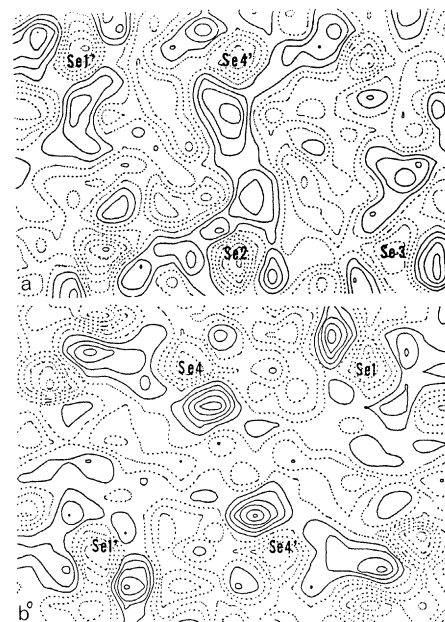


Fig. 4. See description of Fig. 5 for details. (a) The 4.151-\AA Se2-Se4' contact (Fig. 5, plane a); (b) the 3.963-\AA Se4-Se4' contact (Fig. 5, plane c).

served along the b axis (perpendicular to the stacking axis; see Fig. 4), the density maps were examined for tangible evidence of electron density between molecules in the a and b crystallographic directions. Inter- and intrastack Se-Se distances are shown in Table 1.

The results shown in Figs. 2 and 3 represent the observation of intermolecular electron densities in the organic metal. Figure 2 shows an intermolecular electron density of $0.2 e/\text{\AA}^3$ halfway between molecules (vector C1-C1' and

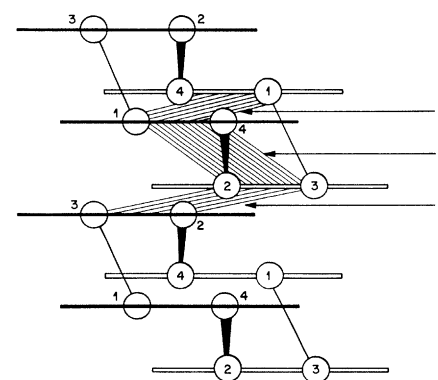


Fig. 5. Schematic view of two stacks of $(\text{TMTSF})_2\text{AsF}_6$. The heavy horizontal lines represent edge-on TMTSF molecules nearest the observer. The lighter horizontal lines represent TMTSF molecules behind the front stack. The numbering arrangement corresponds to that of Figs. 2 and 3 and Table 1. Open circles are front seleniums on the back stack. Numbers outside circles refer to the back stack. Anion octahedra were omitted for clarity. Shaded planes a and c correspond to slices of electron density shown in Fig. 4, a and b, respectively.

C2/C3–C6' in Fig. 2 and vector Se1–Se3'' and Se2''–Se4 in Fig. 3). Figure 2 is a "slice" taken through the bisector of the TMTSF stack (mirror plane bisecting bonds C7–C8 and C2–C3 along the C1–C6 bond), and Fig. 3 is a slice through a plane made up of selenium atoms on the right-hand side of a stack of TMTSF molecules (see Fig. 1).

Examination of Figs. 2 and 3 shows considerable electron density in an alternating pattern between TMTSF molecular centers and between selenium atoms at the edge of adjacent stacks. The alternating intrastack density appears to be an extension of the possible transannular selenium bonding or overlap of appropriate Se–C–Se atomic orbitals and could be considered a microscopic view of electron density distribution along a one-dimensional conduction band.

In order to locate electron density between stacks, it was assumed that electron transfer would be accomplished through the selenium atoms, as suggested earlier (8). Therefore, electron densities in the interstack planes a and c of Fig. 5 were calculated and are depicted in Fig. 4, a and b, respectively.

Surprisingly, and contrary to interactions depicted previously (8), electron density was observed only along the longest Se–Se interstack distance (15) (Se2–Se4', 4.151 Å) as shown in Fig. 4a defined by the atoms Se1', Se4', Se2, and Se3. Aside from the repulsive force of the opposing Se–Se lone-pair density, there is a continuum of density from one molecule to the other which may represent a conduction band. Similar interstack bonding through sulfur lone pairs was postulated for (SN)_x (16). In contrast, in the shortest selenium atom contact (Se2–Se2', 3.905 Å), no electron density is observed in the intermolecular plane (11). The next largest interstack selenium distance is 3.963 Å and corresponds to Se4–Se4'. In this case, even though the selenium atom lone pairs are pointed toward each other, there is no intermolecular continuum of density (Fig. 4b, plane defined by atoms Se1, Se4 and Se1', Se4').

We have shown that there exists intermolecular bonding both within stacks and between stacks in (TMTSF)₂AsF₆ and (TMTSF)₂PF₆. The intermolecular bonding electrons originate from the selenium atoms. One of the proposed four possible modes of interstack selenium bonding is supported by this experimental determination of electron density represented schematically in Fig. 5 (17).

Our results are in accord with previous suggestions concerning the dimensionality of the Bechgaard phase and obser-

Table 1. Intermolecular Se–Se contacts to 5.0 Å.

Atom 1	Atom 2	Distance	Symmetry code*
Se1	Se2	4.053	(-1 1 1 1)
Se1	Se2	4.128	(-1 2 1 1)
Se1	Se3	4.026	(-1 1 1 1)
Se1	Se3	3.874	(-1 2 1 1)
Se1	Se4	3.945	(-1 1 2 1)
Se2	Se2	3.905	(-1 2 0 1)
Se2	Se3	4.977	(-1 2 1 1)
Se2	Se4	4.151	(-1 0-1 0)
Se2	Se4	3.970	(-1 1 1 1)
Se2	Se4	3.919	(-1 2 1 1)
Se4	Se4	3.963	(-1 1 2 1)

The symmetry code $nijk$ denotes the symmetry operation $n^(x, y, z) + (i, j, k)$. For example, the code (-1 1 1 1) corresponds to $(-x, -y, -z) + (1, 1, 1)$ or $(1-x, 1-y, 1-z)$. Intrastack close contacts will have codes of (-1 1 1 1) or (-1 2 1 1). The remaining codes are for various interstack contacts.

vations of magnetotransport (18) in (TMTSF)₂PF₆. This experimental electron density study of an organic metal shows bonding and lone-pair density for selenium atoms along with possible conduction band electrons.

F. WUDL*

D. NALEWAJEK†

Bell Laboratories,
Murray Hill, New Jersey 07974

J. M. TROUP

M. W. EXTINE

Molecular Structure Corporation,
3304 Longmire Drive,
College Station, Texas 77840

References and Notes

1. K. Bechgaard and D. Jerome, *Sci. Am.* **247**, 52 (July 1982).
2. R. M. Metzger, *Mol. Cryst. Liq. Cryst.* **85**, 57 (1982).
3. A. N. Bloch, cited in (2); S. Mazumdar and A. N. Bloch, preprint.
4. P. Coppens, *Int. Rev. Sci.; Inorg. Chem. Ser. Two* **11** 21 (1975).
5. J. M. Troup and R. F. Ziolo, *J. Am. Chem. Soc.* **105**, 229 (1983).
6. M. W. Extine and J. M. Troup, in preparation.
7. J. M. Troup, M. W. Extine, R. F. Ziolo, in *Proceedings of the American Chemical Society*

Symposium on Electron Distribution and the Chemical Bond, M. B. Hall and P. Coppens, Eds. (Plenum, New York, 1982), p. 285.

8. F. Wudl, *J. Am. Chem. Soc.* **103**, 7064, (1981).
9. Electron distribution in the inorganic superconductor V₃Si at room temperature has been determined. This solid, however, is not a molecular crystal and all atoms are covalently bonded to each other. J.-L. Staudenmann, P. Coppens, J. Muller, *Solid State Commun.* **19**, 29 (1976).
10. Low-temperature data are better in terms of the possible $\sin\theta/\lambda$ cutoff than room temperature data, but the differences are minor and affect only the quantitative aspects of the electron density. In our study, the generation of large peaks around the selenium atoms at low temperature (possibly resulting from thermally induced disorder) is far less desirable than the minor quantitative advantages gained at low temperatures. Some common sense is required in the interpretation of what is an artifact of the experiment and what is "real" electron density. In five crystals examined at different temperatures, some features are always present and are probably correct; other features are created or changed from crystal to crystal at low temperatures and cannot be accepted as real electron density features.
11. Full experimental details including additional electron density maps will be part of a full account to be published elsewhere (F. Wudl, D. Nalewajek, E. Aharon-Shalom, J. M. Troup, M. W. Extine, in preparation).
12. D. W. J. Cruickshank, *Acta Crystallogr.* **2**, 65 (1949).
13. An argument could be made that sp^2 and sp^3 -like electron distributions could not be distinguished by examining electron densities because one could take a linear combination of atomic orbitals to give any observed electron density distribution. However, in this case, the absence of electron density in the molecular plane, coupled with the observation of substantial electron density at an angle above and below the plane, is most easily interpretable in terms of symmetry substantially different from sp^2 .
14. W. K. Musker, T. L. Wolford, P. B. Roush, *J. Am. Chem. Soc.* **100**, 6416 (1978); K.-D. Asmus, D. Bahnmann, Ch.-H. Fischer, D. Weltwisch, *ibid.* **101**, 5322 (1979). These authors found transannular S–S bonding in radical cations. It has not been established whether d orbitals are involved.
15. Computations by P. M. Grant led to the same conclusion, independent of the result reported here [P. M. Grant, *Phys. Rev. B* **26**, 6888 (1982)].
16. M. J. Cohen, A. F. Garito, A. J. Heeger, A. G. Mac Diarmid, C. M. Mikulski, M. S. Saran, J. Klipinger, *J. Am. Chem. Soc.* **98**, 3844 (1976).
17. Figure 2 in (8) should be modified accordingly.
18. J. F. Kwak, J. E. Schirber, R. L. Greene, E. M. Engler, *Mol. Cryst. Liq. Cryst.* **79**, 111 (1982).
19. We are particularly indebted to C. K. N. Patel, W. M. Walsh, Jr., and G. A. Thomas for support of this study. We also thank E. A. Chandross for support and Z. Berkovitch-Yellin for critical reading of the manuscript.

* Present address: Department of Physics, University of California, Santa Barbara 93106.

† Present address: Allied Corporation, Buffalo, N.Y. 14210.

28 February 1983; accepted 26 May 1983

Angiotensinogen Is Related to the Antitrypsin-Antithrombin-Ovalbumin Family

Abstract. *The recently reported amino acid sequence of rat angiotensinogen was subjected to a computer-assisted search for homology with known sequences stored in a data bank and found to be significantly related to that of plasma α_1 -antitrypsin, itself a member of a family that includes antithrombin III and ovalbumin. An alignment of the four sequences shows indisputably the common ancestry of all four proteins.*

I have been screening all newly published amino acid sequences as they appear in the literature to see if they resemble sequences of proteins already in my collection (1). Ohkubo and colleagues (2) have recently determined the comple-

mentary DNA (cDNA) sequence for the rat angiotensinogen gene and deduced the amino acid sequence of the protein. The gene encodes a preprotein of 477 residues that includes a 24-residue signal peptide. The mature protein, after re-